Article

Imaging Fast Calcium Currents beyond the Limitations of Electrode Techniques

Nadia Jaafari,[1,2,3] Michel De Waard,[1,3] and Marco Canepari[1,2,3,*]

[1]Institut national de la santé et de la recherche médicale, Grenoble Institute of Neuroscience, Grenoble, France; [2]Université Joseph Fourier, Laboratoire Interdisciplinare de Physique (Centre National de la Recherche Scientifique UMR 5588), France; and [3]Laboratories of Excellence, Ion Channel Science and Therapeutics, France

ABSTRACT The current understanding of Ca^{2+} channel function is derived from the use of the patch-clamp technique. In particular, the measurement of fast cellular Ca^{2+} currents is routinely achieved using whole-cell voltage-clamp recordings. However, this experimental approach is not applicable to the study of local native Ca^{2+} channels during physiological changes of membrane potential in complex cells, since the voltage-clamp configuration constrains the membrane potential to a given value. Here, we report for the first time to our knowledge that Ca^{2+} currents from individual cells can be quantitatively measured beyond the limitations of the voltage-clamp approach using fast Ca^{2+} imaging with low-affinity indicators. The optical measurement of the Ca^{2+} current was correlated with the membrane potential, simultaneously measured with a voltage-sensitive dye to investigate the activation of Ca^{2+} channels along the apical dendrite of the CA1 hippocampal pyramidal neuron during the back-propagation of an action potential. To validate the method, we analyzed the voltage dependence of high- and low-voltage-gated Ca^{2+} channels. In particular, we measured the Ca^{2+} current component mediated by T-type channels, and we investigated the mechanisms of recovery from inactivation of these channels. This method is expected to become a reference approach to investigate Ca^{2+} channels in their native physiological environment.

INTRODUCTION

The measurement of ionic currents in single-electrode and two-electrode voltage-clamp experiments implies that the cell is maintained at a given membrane potential (V_m) by compensating the cell current (1). The current measured with the electrode is the summation of the filtered currents from all different cellular regions, including remote regions where V_m is unclamped (2). To study the function of native channels, including those expressed under pathological conditions, ionic currents should be recorded at the site of origin during physiological changes of V_m. Local current measurements from a limited number of cellular sites can be obtained using dendritic patch-clamp recordings with one electrode (3) or two electrodes at the same site (2), but even if the V_m is dynamically clamped locally, this will never correspond to a physiological V_m change occurring in the cell. The limitation of the voltage-clamp approach, for a Ca^{2+} current (I_{Ca}), may in principle be overcome by an independent optical measurement of the current at the locus of its origin using fluorescence Ca^{2+} indicators. In an important reference study (4), Kao and Tsien proposed that in the presence of an endogenous cellular Ca^{2+} buffer, the relaxation time of the dye-Ca^{2+} binding reaction (τ_R) can be approximated by the equation

$$\tau_R = \frac{1}{K_{ON}^{Dye} \times [Ca^{2+}] + K_{OFF}^{Dye}}, \quad (1)$$

where K_{ON}^{Dye} and K_{OFF}^{Dye} are the association and dissociation constants of the reaction, respectively. In general, for Ca^{2+} indicators, the association constant is fast and limited by diffusion between $2 \times 10^8\ M^{-1}\ s^{-1}$ and $6 \times 10^8\ M^{-1}\ s^{-1}$. The equilibration time of the reaction is therefore mainly determined by the dissociation constant, i.e., by the equilibrium constant (K_D) that varies from indicator to indicator, determining the affinity to Ca^{2+} (4). As shown in Fig. S1 in the Supporting Material, this relaxation time is <1 ms for low affinity indicators with $K_D > 10\ \mu M$, suggesting the possibility of using these indicators for the measurement of a fast I_{Ca}.

In Ca^{2+} imaging recordings, the fractional change of fluorescence ($\Delta F/F_0$) is proportional to the change of Ca^{2+} ions bound to the indicator ($[DCa^{2+}]$) (5). If $[DCa^{2+}]$ is also proportional to the total free Ca^{2+} concentration entering the cell through the plasma membrane ($[Ca^{2+}]_{TOT}$), then I_{Ca} at its site of origin can be extrapolated, in theory, by the derivative of $\Delta F/F_0$ ($d\Delta F/F_0/dt$). This scenario may occur if the equilibration of the dye-Ca^{2+} binding reaction is faster than the rise time of I_{Ca}, which is possible, in principle, with low-affinity indicators (6). The possibility of measuring I_{Ca} optically was theoretically explored by Sabatini and Regehr (7). In that study, a fast Ca^{2+}-$\Delta F/F_0$ measurement from multiple axons was

Submitted March 25, 2014, and accepted for publication July 30, 2014.

*Correspondence: marco.canepari@ujf-grenoble.fr

Editor: Brian Salzberg

0006-3495/14/09/1280/9 $2.00

http://dx.doi.org/10.1016/j.bpj.2014.07.059

converted into an optical measurement of I_{Ca}, but without an experimental validation, which requires single-cell resolution and the combined possibility to record the current with an electrode. This validation is crucial, since the possibility of extracting I_{Ca} from the Ca^{2+}-$\Delta F/F_0$ signal requires two additional conditions. First, the Ca^{2+} bound to the indicator must be proportional to the Ca^{2+} bound to the cell native buffers during the whole Ca^{2+} influx process; in particular, Ca^{2+} sequestration by slow endogenous buffers must be negligible during the current, since these mechanisms would decrease $\Delta F/F_0$ independently of $[Ca^{2+}]_{TOT}$. Second, Ca^{2+} release from internal stores should be negligible during the current.

Here, we addressed this challenge using a believed novel technology, and we demonstrate experimentally the possibility of recording calcium currents (I_{Ca}) by Ca^{2+} imaging experiments, achieving these measurements from distinct subcellular regions of individual neurons. In particular, we measured fast I_{Ca} volume densities mediated by voltage-gated Ca^{2+} channels during physiological changes of V_m,using the low-affinity indicator Oregon Green 488 BAPTA-5N (8,9). The optical measurement of the I_{Ca} was also correlated with V_m, which was simultaneously measured with the intracellularly loaded voltage-sensitive dye JPW1114 (10), allowing exploration of voltage-dependence properties of native Ca^{2+} channels.

MATERIALS AND METHODS

Slice preparation, solutions, and electrophysiology

Experiments were approved by the Isere prefecture (authorization no. 38 12 01) and the specific protocol (no. 197) by the ethics committee of the Grenoble Institute of Neuroscience. As previously described (11), hippocampal slices (250 μm thick) were prepared from 21- to 35-day postnatal C57Bl6 mice using a VF-200 Compresstome (Precisionary Instruments, Greenville, NC). Slices were cut in iced extracellular solution and incubated at 37°C for 1 h before use. The extracellular solution used contained (in mM) 1 $MgSO_4$, 125 NaCl, 26 $NaHCO_3$, 20 glucose, 3 KCl, 1 NaH_2PO_4, and 2 $CaCl_2$ bubbled with 95% O_2 and 5% CO_2. The intracellullar solution contained (in mM) 125 $KMeSO_4$, 5 KCl, 8 $MgSO_4$, 5 Na_2-ATP, 0.3 Tris-GTP, 12 Tris-phosphocreatine, and 20 HEPES, adjusted to pH 7.35 with KOH. To block Na^+ and K^+ channels in voltage-clamp experiments, the external solution also contained 1 μM tetrodotoxin, 5 mM tetraethylammonium, 4 mM 4-aminopyridine, and 250 nM apamin, and the internal solution also contained 5 mM tetraethylammonium. Ca^{2+} indicators were added at a concentration of 1 mM. In voltage-imaging experiments, cells were loaded as previously described (12) with the voltage-sensitive dye JPW1114, which was present in the patch pipette at a concentration of 120 μg/mL. In experiments with BAPTA, the internal solution also contained 300 μM EGTA, to prevent a possible decrease of the basal free BAPTA concentration. In experiments with NP-EGTA, the internal solution also contained 150 μM $CaCl_2$, to begin with a free Ca^{2+} concentration equal to the K_D of NP-EGTA. Indicators and chelators were purchased from Invitrogen (Carlsbad, CA). All other chemicals were purchased either from Tocris (Bristol, UK) or Sigma-Aldrich (St. Louis, MO). Experiments were performed at 32°C using an Olympus (Tokyo, Japan) BX51 microscope equipped with a 60×/1.0 NA Nikon (Tokyo, Japan) objective. Patch-clamp recordings were made using a multiclamp amplifier (700A, Molecular Devices, Sunnyvale, CA), and voltage and current signals were acquired with the A/D board of the charge-coupled device (CCD) camera. The V_m measured with the patch pipette was corrected for the junction potential (−11 mV), as previously estimated (13). In voltage-clamp recordings, I_{Ca} was evoked by depolarizing pulses from −70 mV to −10 mV and measured in the soma by subtracting the scaled subthreshold current associated with a voltage step from −70 mV to −10 mV.

The imaging system

Simultaneous ultraviolet (UV)/blue LED illumination from the epifluorescence port of the microscope was allowed by a 409 nm dichroic mirror (FF409, Semrock, Rochester, NY). The 365 nm LED used for photolysis was controlled by an OptoFlash (Cairn Research, Faversham, United Kingdom) and the 470 nm other LED used for fluorescence excitation was controlled by an OptoLED (also from Cairn). The demagnification of the image and the separation of the two emission wavelengths were done with a previously described system (14). The two images were acquired with a dual-head NeuroCCD-SMQ camera (RedShirtimaging, Decatur, GA) at 510 ± 42 nm (for Ca^{2+}) and at >610 nm (for V_m). The demagnifications of the two aligned images were 0.5×, 0.25×, and 0.125×. At 0.125×, it was not possible to obtain the same focal plane for the two images, so this configuration was used only for individual Ca^{2+} imaging. Although the camera has 80 × 80 pixels per head (full resolution), to achieve a speed of 20 kHz, binned stripes of 26 × 4 pixels were imaged. In contrast to previous reports (13,15), JPW1114 was excited at 470 nm and not at 532 nm, since this wavelength corresponds to the peak of OG5N emission. The sensitivity of the voltage-sensitive dye at 470 nm was around four times less than that at 532 nm. In neurons loaded with only one indicator, either OG5N or JPW1114, the signals detected by the CCD head devoted to the recording of fluorescence from the other indicator were negligible. Thus, it was possible to unambiguously discriminate Ca^{2+} fluorescence from V_m fluorescence.

Recording and analysis of Ca^{2+} and V_m optical signals

Ca^{2+} recordings were made at 20 kHz, starting 20–25 min after establishing the whole-cell configuration. This time was necessary to achieve equilibration of the indicator over the dendritic segment of recording (Fig. S2 *a*). To attain a good signal/noise ratio (S/N), fluorescence was averaged over 16–64 trials, as specified in each figure legend. Individual trials were saved in separate files and averaged offline. In this way, series of trials where the kinetics of the action potential changed during the sequence were discarded. The $\Delta F/F_0$ signal was calculated without subtraction of the autofluorescence background. The dendritic fluorescence in cells loaded with 1 mM OG5N 25 min after establishing the whole-cell configuration decreased with the distance from the soma, as shown in Fig.S2 *b*. In particular, in the first 100 μm apical segment, dendritic fluorescence was always more than three times larger than autofluorescence estimated in large adjacent regions, with a variability of ~15% from cell to cell at the same distance from the soma. This test shows that the contribution of autofluorescence was not critical for the empirical estimates of the Ca^{2+} currents in the proximal apical dendritic regions obtained with the two calibration procedures.

Fluorescence averages were also corrected for bleaching using trials without signal. To achieve a good S/N in the $d(\Delta F/F_0)/dt$ signal, we applied a Savitzky-Golay filter (16) to the $\Delta F/F_0$ signal before differentiation. The filter was implemented by the smooth function in the Matlab (The Mathworks, Natick, MA) Curve Fitting Toolbox. In all data reported here, the OG5N-$\Delta F/F_0$ signal was smoothed using a filter window of 20–30 samples. This filter did not produce any temporal distortion. The Savitzky-Golay filter proved to be the best algorithm to improve the S/N of the $d(\Delta F/F_0)/dt$ signal, as described in Fig. S3. Its implementation, however,

required signal oversampling, which motivated our choice to record fluorescence at the highest possible rate of the camera (20 kHz).

The JPW1114-$\Delta F/F_0$ signal was always calibrated in terms of V_m change on an absolute scale using a previously demonstrated protocol, based on wide-field photorelease of L-glutamate from the caged compound 4-methoxy-7-nitroindolinyl-caged-L-glutamate (MNI-glutamate) (15). Briefly, a calibration of the JPW1114-$\Delta F/F_0$ signal can be done if an electrical signal of known amplitude is available at all recordings sites (12,17). In many neuronal types, activation of a large portion of ionotropic glutamate receptor makes them the dominant conductance and the resulting V_m will be 0 mV in all the illuminated area. Thus, by activation of >50% of the AMPA receptors with glutamate uncaging starting from the resting V_m, we were able to calibrate the JPW1114-$\Delta F/F_0$ signal that corresponded to a change of V_m from the resting V_m to 0 mV.

RESULTS

Low-affinity Ca^{2+} indicators are capable of tracking fast Ca^{2+} currents

The straightforward strategy to test whether I_{Ca} can be derived from a $\Delta F/F_0$ Ca^{2+} signal is to compare the kinetics of $\Delta F/F_0$ signal with that of the I_{Ca} integral ($\int I_{Ca}$). To this purpose, we performed patch-clamp recordings from CA1 hippocampal pyramidal neurons in slices of the mouse brain filled with a Ca^{2+} indicator, using an imaging system capable of recording at the frame rate of 20 kHz. We measured I_{Ca} evoked by depolarizing pulses from −70 mV to −10 mV in the presence of Na^+ and K^+ channels blockers (see Materials and Methods). With the Ca^{2+} indicator in the patched pipette at 1 mM concentration, we simultaneously recorded $\Delta F/F_0$ from the initial 60 μm apical dendritic segment (Fig. 1 *a*). Thus, under these pharmacological conditions, the voltage step depolarized this proximal dendritic region to ~−10 mV for the first 4 ms, a time interval sufficient to explore the fast kinetics of the Ca^{2+} influx (see Fig. S4).

The rate of the dye-Ca^{2+} reaction depends on the affinity (K_D) of the indicator. In that respect, low-affinity indicators ($K_D > 10$ μM) can equilibrate in hundreds of microseconds (18). Thus, in these experiments, we performed a proof-of-principle test on the high-affinity indicator Oregon Green 488 BAPTA-1 (OGB1, K_D = 206 nM (19)) and on the low-affinity indicator Oregon Green 488 BAPTA-5N (OG5N, K_D = 35–46 μM (8,9)). Fig. 1 *b* shows two representative examples of $\Delta F/F_0$ kinetics and of the associated $\int I_{Ca}$ where the two curves were normalized to 1 over the first 4 ms. The $\int I_{Ca}$ curve matched the $\Delta F/F_0$ curve with OG5N, but not with OGB1. To quantify the match between the two curves for the two indicators, we computed the area of their difference (S), which was positive for OGB1 and nearly 0 for OG5N (Fig. 1 *c*). In two groups of cells, the area of the difference between $\int I_{Ca}$ and $\Delta F/F_0$ was 0.19 ± 0.03 (N = 5 cells) for OGB1, significantly different ($p < 0.01$, two-population *t*-test) from the values obtained for OG5N (0.01 ± 0.02, N = 12 cells). Since OG5N-$\Delta F/F_0$ is proportional to the associated $\int I_{Ca}$, its derivative must be also proportional to I_{Ca}. In the representative example of Fig. 1 *d*, the $d(\Delta F/F_0)/dt$ was calculated after smoothing the $\Delta F/F_0$ signal using a Savitzky-Golay filter (16) (Fig. 1 *e*). This demonstrates that the low-affinity indicator OG5N is adequate for tracking I_{Ca} in time.

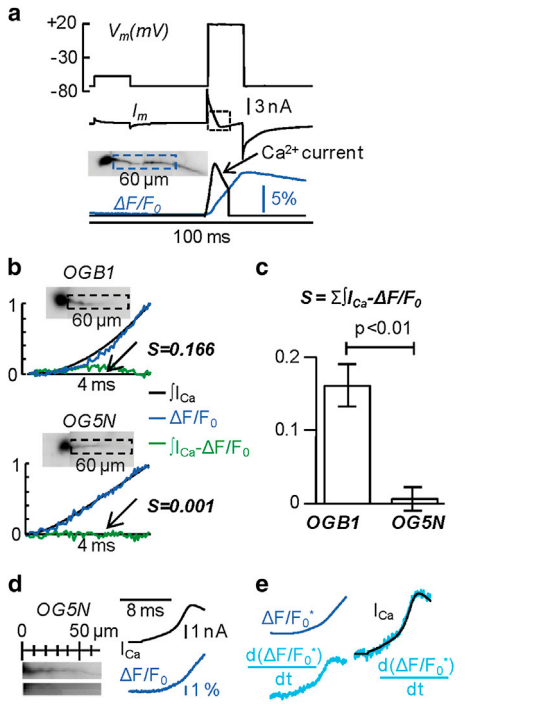

FIGURE 1 The change of fluorescence of OG5N matches the integral of a Ca^{2+} current. (*a*) Voltage-clamp protocol on a CA1 hippocampal pyramidal neuron (*inset*) consisting of two 16 ms voltage pulses from −70 mV, the first to ~−60 mV below the threshold for activation of Ca^{2+} channels and the second to ~20 mV. Experiments were performed in the presence of Na^+ and K^+ channel blockers. I_{Ca} (*Ca^{2+} current*) was extracted by subtraction of the scaled current associated with the subthreshold pulse minus the current associated with the larger-voltage pulse for the period defined by the dotted box. The kinetics of the current were analyzed in correlation with that of the $\Delta F/F_0$ signal in the initial 60 μm segment of the apical dendrite (*gray trace*). (*b*) Two neurons filled either with OGB1 or OG5N (*insets*), with the $\int I_{Ca}$ (*black*) and Ca^{2+} $\Delta F/F_0$ (*blue*) normalized to their maxima. Differences between the two curves ($\int I_{Ca}$ − $\Delta F/F_0$) are also reported. The surface of this difference (*S*) is indicated. (*c*) Mean ± SD of S for OGB1 and OG5N. Values of S are significantly different (two-population *t*-test, $p < 0.01$). (*d*) Voltage-clamp measurement of I_{Ca} (average of 16 trials) with OG5N, showing the I_{Ca} measurement with the patch electrode (*upper*) and the associated $\Delta F/F_0$ from the initial 60 μm apical dendritic segment (*lower*). (*e*) Filtered $\Delta F/F_0$ ($\Delta F/F_0$*, *upper left*) and its derivative (*lower left*). At right, the $\Delta F/F_0$* derivative is superimposed on the I_{Ca} trace. To see this figure in color, go online.

Extraction of local Ca^{2+} current volume densities from Ca^{2+} fluorescence changes

Based on the above calculations, differentiation of the OG5N-$\Delta F/F_0$ signal can provide a signal with the same kinetics observed for I_{Ca}, allowing local currents to be measured regionally during a physiological change of V_m.

However, this situation applies only if two additional conditions are met. First, binding to endogenous Ca^{2+} buffers that are slower than OG5N and Ca^{2+} extrusion should be negligible during the entire I_{Ca}, since these two mechanisms decay $\Delta F/F_0$, producing a negative component of $d\Delta F/F_0/dt$. Second, Ca^{2+} release from stores should not contribute to $[Ca^{2+}]_{TOT}$, since this would distort the rise of $\Delta F/F_0$ with respect to the Ca^{2+} influx through the plasma membrane. Fig. 2 *a* shows an example of $\Delta F/F_0$ associated with an action potential from the most proximal dendritic segment (0–60 μm from the soma) obtained with OG5N. The $\Delta F/F_0$ onset occurred before the action potential peak and its slope was nearly zero for a few milliseconds after the peak. According to the time course of $\Delta F/F_0$, $d\Delta F/F_0/dt$ reaches its peak at the time of $\Delta F/F_0$ maximal slope and returns to zero. We then repatched the cell with additional 40 μM BAPTA, which is a high-affinity buffer and has slower kinetics compared to OG5N. Thus, BAPTA mimics the presence of an endogenous Ca^{2+} buffer that would be capable of distorting the $d\Delta F/F_0/dt$.

After addition of BAPTA, the $\Delta F/F_0$ decayed more rapidly after the peak, introducing a small negative component to $d\Delta F/F_0/dt$ (Fig. 2 *a*). This observation shows that a flat $\Delta F/F_0$ slope after the peak is the indication that both binding to slow endogenous Ca^{2+} buffers and Ca^{2+} extrusion occur less rapidly than Ca^{2+} influx. To exclude Ca^{2+} release from stores during the action potential, we blocked ryanodine receptors with 200 μM ryanodine (20), inositol triphosphate ($InsP_3$) receptors with 100 μg/mL heparine (21), and phospholipase-C and $InsP_3$ formation with 5 μM U73122 (22). The representative cell in Fig. 2 *b* was first patched with the control internal solution and, sequentially, with inhibitors of Ca^{2+} release from stores. These had no effect on $\Delta F/F_0$ or on its derivative. This result was consistent in the four cells tested, indicating that Ca^{2+} release from stores doesn't occur during the action potential.

The previous result demonstrates that the OG5N-$\Delta F/F_0$ signal associated with an action potential is exclusively due to Ca^{2+} influx through the plasma membrane. It follows that the $d\Delta F/F_0/dt$ signal can be, in principle, converted into I_{Ca} volume density (I_{Ca}/V) by estimating the $[Ca^{2+}]_{TOT}$ corresponding to a given OG5N-$\Delta F/F_0$ signal. An accurate estimate of I_{Ca}/V in the initial apical dendritic segment was obtained using two independent procedures. In the first procedure, we filled eight cells with a solution in which 300 μM NP-EGTA (23) and 150 μM $CaCl_2$ were added. NP-EGTA is a photolabile chelator that selectively binds Ca^{2+} with high affinity and releases it rapidly upon photolysis in an irreversible manner. Under these conditions, a depolarization from -70 to -10 mV produced a persistent OG5N-$\Delta F/F_0$ signal of >20% in the most proximal 80 μm of the dendrite (Fig. 3 *a*), and a further depolarization step

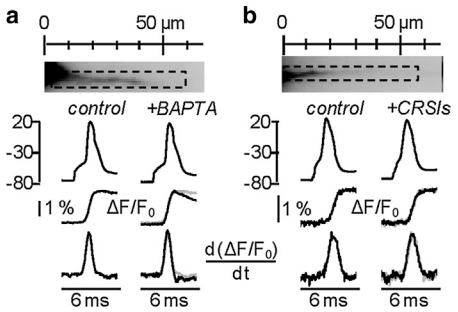

FIGURE 2 Ca^{2+} sequestration by slow endogenous buffer and Ca^{2+} release from stores are negligible during an action potential. (*a*) The neuron is patched first with control solution plus 300 μM EGTA and OG5N and sequentially with an additional 40 μM BAPTA. Shown are an action potential (*upper*), the associated $\Delta F/F_0$ (*middle*), and $d\Delta F/F_0/dt$ (*lower*). Addition of BAPTA speeds up the decay of $\Delta F/F_0$, introducing a negative component to $d\Delta F/F_0/dt$. In the BAPTA column, the control signal is superimposed in gray. (*b*) Same protocol as in *a*, with the neuron patched first with control solution and later with added inhibitors of Ca^{2+} release from stores (CRSIs). $\Delta F/F_0$ and $d\Delta F/F_0/dt$ do not change after addition of CRSIs. In the CRSIs column, the control signal is superimposed in gray. Data are from averages of 32 trials.

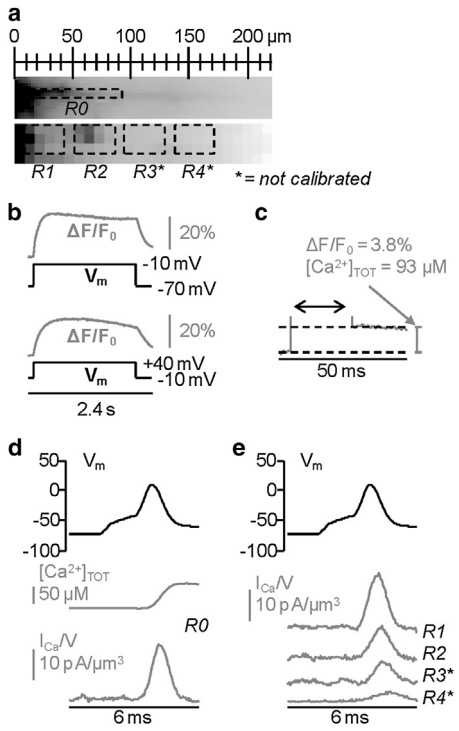

FIGURE 3 I_{Ca}/V calibration using NP-EGTA. (*a*) Full-resolution and binned-resolution images of the apical dendrite, highlighting the region of calibration (*R0*) and additional regions of interest (*R1–R4*). The calibration does not apply to *R3* and *R4*. (*b*) OG5N-$\Delta F/F_0$ from R0 associated with a voltage step from -70 mV to -10 mV (*upper*) and another voltage step from -10 mV to $+40$ mV (*lower*). (*c*) $\Delta F/F_0$ (*gray*) with a peak of 3.8% was associated with photorelease of 93 μM Ca^{2+} from NP-EGTA by fitting the signals of a sequence of 16 pulses to Eq. 2. (*d*) From the same cell, the $\Delta F/F_0$ associated with an action potential (*black*) was filtered and differentiated (*gray*). The I_{Ca}/V was obtained from the $d(\Delta F/F_0/dt)$ using the calibration described in *a*. Data are from averages of 64 trials. (*e*) Using the calibration in *a*, the I_{Ca}/Vs from regions R1–R4 associated with an action potential are shown.

of +50 mV produced an additional OG5N-$\Delta F/F_0$ signal of >20% (Fig. 3 *b*). Since the K_D of NP-EGTA before photolysis is 80 nM (23) and the K_D of OG5N is 35 μM (8), the large and persistent OG5N-$\Delta F/F_0$ increase from −70 to −10 mV indicates that all NP-EGTA is bound to Ca^{2+} at −10 mV. The further increase of OG5N-$\Delta F/F_0$ from −10 to +40 mV demonstrates that OG5N is still not saturated at −10 mV. Although $V_m = -10$ mV, 300 μM Ca^{2+} is available for uncaging, and a sequence of pulses will progressively release Ca^{2+} until all NP-EGTA is photolysed, i.e., until the whole 300 μM Ca^{2+} is released. Thus, we performed the calibration by applying a sequence of 16 UV pulses (20 ms) and measuring the OG5N-$\Delta F/F_0$ signal every 5 s. The Ca^{2+} released at pulse *k* follows the geometric progression (24)

$$[Ca^{2+}]_{TOT}(k) = \alpha \times \left(300\ \mu M - \sum_{j=0}^{k-1}[Ca^{2+}]_{TOT}(j)\right), \quad (2)$$

where α is the photolytic conversion per UV pulse. In the cell of Fig. 3 *a*, an OG5N-$\Delta F/F_0$ signal of 3.8% corresponded to $[Ca^{2+}]_{TOT} = 93$ μM (Fig. 3 *c*). The $[Ca^{2+}]_{TOT}$ associated with an action potential was converted into a charge/volume ratio (Q/V) using the equation

$$Q/V = \frac{[Ca^{2+}]_{TOT} \times 2e \times N_A}{dm^3}, \quad (3)$$

where *e* is the fundamental charge, dm is the decimeter unit and N_A is the Avogadro number (Fig. 3 *d*). The smoothed signal was differentiated and expressed as I_{Ca}/V. The current was obtained by converting $[Ca^{2+}]_{TOT} = 1$ μM to an equivalent charge volume density of 1.9297×10^{-4} pC/μm^3. By assuming a uniform conversion factor for the sites included in the calibrating region (most proximal 80 μm dendrite), I_{Ca}/V could be estimated (Fig. 3 *e*). In the more distal regions, the $d\Delta F/F_0/dt$ signal has the same kinetics as the I_{Ca}, but is not calibrated. In the eight cells analyzed in this way, the OG5N-$\Delta F/F_0$ signal of 1% corresponded to a $[Ca^{2+}]_{TOT}$ of 20 ± 3 μM.

In the second procedure, applied to six cells, we sequentially patched the neuron first with 1 mM OG5N in the pipette and later with an additional 40 μM of the high-affinity chelator BAPTA. As expected from Eq. 1, addition of the higher-affinity chelator BAPTA, which is slower than OG5N in equilibrating, has a negligible effect on the fast peak of the OG5N-$\Delta F/F_0$ signal (Fig. 2 *a*). However, BAPTA sequestrates Ca^{2+} both from OG5N and from the endogenous buffer during its slower equilibration, changing the decay of the OG5N-$\Delta F/F_0$ signal. If BAPTA is saturated, the difference between the OG5N-$\Delta F/F_0$ signal before and after addition of BAPTA must correspond to a $[Ca^{2+}]_{TOT}$ equal to the BAPTA concentration. We investigated the OG5N-$\Delta F/F_0$ signal associated with four action potentials elicited at 5 ms intervals in control conditions and after repatching the cell with the solution containing BAPTA, as shown in the cell in Fig. 4 *a*. The OG5N-$\Delta F/F_0$ peak associated with the first action potential had nearly the same peak in control solution as in the solution with BAPTA, but the OG5N-$\Delta F/F_0$ peak associated with the next action potentials was larger in the control solution, and the difference between the OG5N-$\Delta F/F_0$ peaks associated with the third and fourth action potentials was nearly the same. We concluded that the difference between OG5N-$\Delta F/F_0$ signals with the two solutions, after the third action potential, corresponded to 40 μM Ca^{2+}. We used this difference for the calibration of I_{Ca}/V at the proximal dendrite (Fig. 4 *b*). In the six cells calibrated with a sequential patch with BAPTA, an OG5N-$\Delta F/F_0$ signal of 1% corresponded to a $[Ca^{2+}]_{TOT}$ of 22 ± 9 μM, similar to that obtained using the first procedure (Fig. 4 *c*). Given these similar results obtained with two different procedures, a standard calibration of OG5N-$\Delta F/F_0$ = 1%, corresponding to $[Ca^{2+}]_{TOT} = 20$ μM, was applied in the proximal dendrite.

Use of optical Ca^{2+} current measurements to study T-type channels

To assess the capability of this believed novel approach to study the behavior of native channels under physiological activity, we investigated the voltage dependence of the I_{Ca}/V

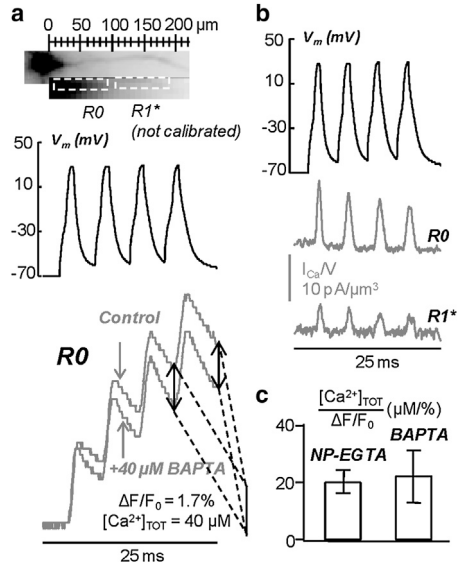

FIGURE 4 Calibration of I_{Ca}/V using BAPTA injection. (*a*) OG5N-$\Delta F/F_0$ signals from the initial 80 μm segment (region R0) of the cell shown above associated with a sequence of four action potentials (*black trace*) at 200 Hz. Recordings were completed under control conditions (1 mM OG5N + 300 μM EGTA) and after repatching the cell with 40 μM BAPTA added to the solution. The difference between the two OG5N-$\Delta F/F_0$ signals corresponds to $[Ca^{2+}]_{TOT} = 40$ μM. (*b*) I_{Ca}/V associated with the a sequence of four action potentials (*black trace*) from regions R0 and R1 in control conditions (*gray traces*). The calibration does not apply to R1. (*c*) The mean ± SD of the $[Ca^{2+}]_{TOT}$/OG5N-$\Delta F/F_0$ ratios obtained using either NP-EGTA or BAPTA. Data are from averages of 32 trials.

associated with action potentials. To this end, we simultaneously monitored V_m optically with the voltage-sensitive dye JPW1114 (14). Initially, we measured I_{Ca}/V and V_m associated with an action potential in the proximal apical dendritic segment (Fig. 5 *a*). I_{Ca}/V and V_m were measured under two conditions: for an action potential starting at $V_m = -60$ mV and for an action potential starting at $V_m = -80$ mV (Fig. 5 *b*). When the action potential started at $V_m = -80$ mV, I_{Ca}/V was larger and started at a more hyperpolarized V_m, indicated as V_m^0 in Fig. 5 *c*. This result, consistent in all the six cells tested (Fig. 5 *d*), suggested that at $V_m = -60$ mV, the I_{Ca} was mediated by different types of high-voltage-activated Ca^{2+} channels expressed in this neuronal type (25), whereas the I_{Ca}/V starting at $V_m = -80$ mV contained a contribution of T-type voltage-gated Ca^{2+} channels (26). To confirm this hypothesis, we tested the combined effect of the specific T-type channel blockers (1*S*,2*S*)-2-[2-[[3-(1*H*-Benzimidazol-2-yl)propyl]methylamino]ethyl]-6-fluoro-1,2,3,4-tetrahydro-1-(1-methylethyl)-2-naphthalenyl-cyclopropanecarboxylate-dihydrochloride (NNC, 30 μM) (27) and 3,5-dichloro-*N*-[[(1α,5α,6-exo,6α)-3-(3,3-dimethylbutyl)-3-azabicyclo[3.1.0]hex-6-yl]methyl]-benzamide-hydrochloride (ML218, 5 μM) (28) and the nonspecific voltage-gated Ca^{2+} channel blocker $CdCl_2$ (100 μM) in separate I_{Ca}/V recordings (Fig. 5, *e* and, *f*).

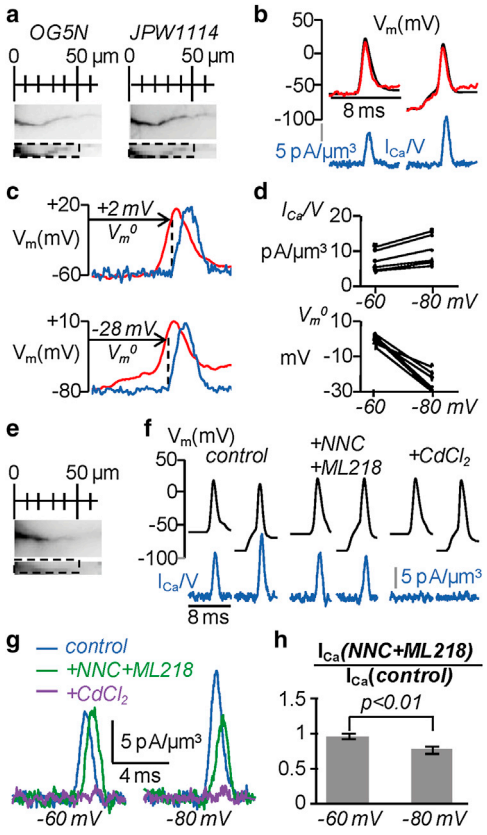

FIGURE 5 Dendritic I_{Ca}/Vs associated with action potentials at different starting V_ms. (*a*) Fluorescence images of a cell filled with OG5N (*left*) and JPW1114 (*right*), shown at full resolution (*upper*) and binned resolution (*lower*). Dashed box indicates the region of interest where fluorescence was averaged. (*b*) I_{Ca}/V associated with one action potential starting either at $V_m = -60$ mV or -80 mV. The V_m recorded optically (*red*) and with the electrode (*black*) are superimposed. (*c*) I_{Ca}/V superimposed on the action potential for the two cases. The V_m at the current onset (V_m^0) is indicated. (*d*) I_{Ca}/V peak and V_m^0 associated with action potentials starting either at $V_m = -60$ mV or $V_m = -80$ mV for six cells. (*e*) Neuron filled with OG5N, with the region of interest outlined. (*f*) I_{Ca}/V associated with action potentials (*black*) starting either at $V_m = -60$ mV or $V_m = -80$ mV under control conditions, after addition of NNC + ML218, and after addition of $CdCl_2$. (*g*) Superimposed I_{Ca}/Vs for the different conditions (inhibition by T-type channel blockers of I_{Ca}/V starting at $V_m = -80$ mV). (*h*) Mean ± SD (N = 7 cells) of I_{Ca}/Vs with NNC + ML218 normalized to control I_{Ca}/V at $V_m = -60$ mV and $V_m = -80$ mV ($p < 0.01$, two-population *t*-test). Data are from averages of 32 trials. To see this figure in color, go online.

As shown in Fig. 5, *f* and *g*, T-type channel blockers inhibit the I_{Ca}/V associated with an action potential starting at $V_m = -80$ mV, but not the I_{Ca}/V associated with an action potential starting at $V_m = -60$ mV. This result was consistent in all the cells tested (Fig. 5 *h*). In seven cells, the mean ± SD of I_{Ca}/V after addition of NNC + ML218, normalized to I_{Ca}/V in control conditions, was 0.96 ± 0.04 at $V_m = -60$ mV and 0.77 ± 0.05 at $V_m = -80$ mV. To further test the efficacy and selectivity of these two relatively new molecules in our preparation, we performed a series of voltage-clamp recordings, measuring both the somatic I_{Ca} and the proximal dendritic I_{Ca}/V associated with 16 ms voltage steps from -80 mV to -20 mV or from -60 mV to 0 mV (Fig. 6 *a*). We performed these two recordings first in control conditions and then after adding NNC and ML218. In this way, we measured for both voltage steps the component, mediated by high-voltage-activated Ca^{2+} channels, of the somatic I_{Ca} and of the dendritic I_{Ca}/V. Both components were blocked by further addition of 100 μM $CdCl_2$, which at this concentration did not bind to the indicator inside the cell. From these measurements, we extracted the T-type channel component of the electrode and optical I_{Ca} by subtracting the signals in the presence of the T-type channel blockers from the control signals (Fig. 6 *b*). A relevant T-type-channel-mediated component of the I_{Ca} was present only when the initial V_m was -80 mV, because at this initial V_m, these channels recover from inactivation. In the six cells tested, the T-type current and the optically measured T-type-current volume density associated with a -80 mV to -20 mV pulse were 1.18 ± 0.48 nA and 1.31 ± 0.60 pA/μm^3, respectively. The same signals associated with a step from -60 mV to 0 mV were 0.25 ± 0.12 and 0.30 ± 0.18 pA/μm^3, respectively.

In conclusion, we confirm using our optical recordings that T-type Ca^{2+} channels are inactivated at $V_m = -60$ mV and that recovery from inactivation by setting the initial $V_m = -80$ mV permits their activation during the action potential.

Next, we investigated from a longer apical dendritic segment the I_{Ca}/V starting from the resting V_m (typically between -70 mV and -60 mV), uniform along the apical

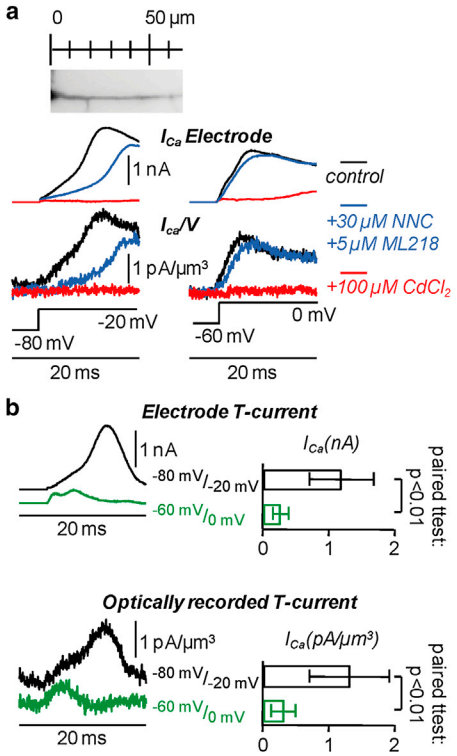

FIGURE 6 Pharmacological tests of T-type channel blockers NNC and ML218 in voltage-clamp experiments. (*a*) (*Upper*) Initial dendritic segment of a CA1 hippocampal pyramidal neuron from experiments performed in the presence of Na^+ and K^+ channels blockers. Fluorescence was averaged over the entire region. (*Lower*) I_{Ca} measured with the patch electrode or optically (I_{Ca}/V), associated with depolarizing pulses from −80 mV to −20 mV or from −60 mV to 0 mV in voltage clamp. Recordings performed in control conditions, in the presence of T-type channel blockers NNC (30 μM) and ML218 (5 μM), and after addition of $CdCl_2$ (100 μM) are represented in different colors. (*b*) Electrode and optical recordings of T-type currents from −80 mV to −20 mV and from −60 mV to 0 mV obtained by subtracting the currents with NNC + ML218 from the control currents. It can be seen at right that the mean ± SD (N = 6 cells) of both electrode and optically recorded T-type currents associated with the two voltage steps were significantly different ($p < 0.01$, paired *t*-test). Data are from averages of 16 trials. To see this figure in color, go online.

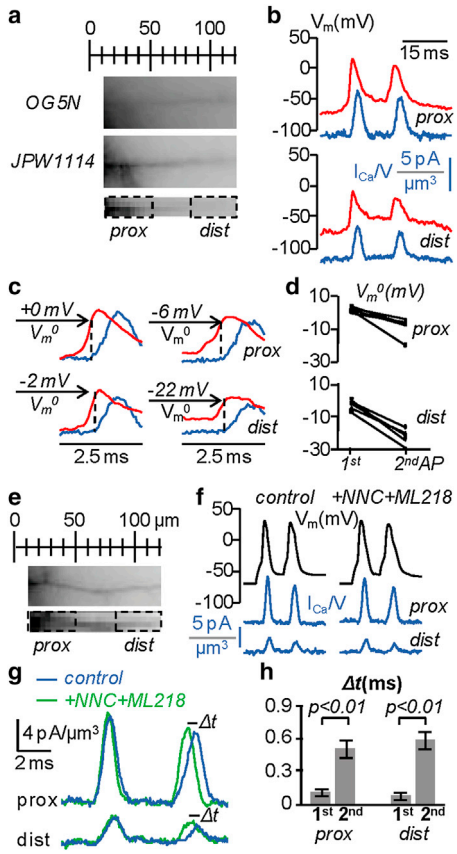

FIGURE 7 Dendritic I_{Ca}/V associated with two action potentials at 200 Hz. (*a*) Cell filled with OG5N and JPW1114 dye, with proximal (*prox*) and distal (*dist*) regions of interest outlined. (*b*) Proximal and distal I_{Ca}/V (*gray*) associated with two action potentials recorded optically (*black*) at 5 ms intervals starting from a resting V_m, which was 67 mV in this particular cell. (*c*) I_{Ca}/V superimposed on the proximal and distal action potentials, with the V_m at the current onset (V_m^0) indicated. (*d*) V_m^0 associated with the proximal and distal action potentials from five cells. (*e*) Neuron filled with OG5N, with proximal and distal regions outlined. (*f*) Proximal and distal I_{Ca}/V (*gray*) associated with two action potentials (*black*) at 5 ms intervals starting from a resting V_m of 68 mV. Recordings were performed in control conditions and after addition of NNC + ML218. (*g*) I_{Ca}/V in control conditions (*gray*) and after addition of T-type channel blockers (*black*). T-type channel blockers delay (Δt) the second I_{Ca}/V with respect to the first. (*h*) Mean ± SD (N = 6 cells) of proximal and distal delays (Δt) produced by addition of T-type channel blockers. The difference in Δt between the first and second action potentials both proximally and distally was significant ($p < 0.01$, two-population *t*-test). Data are from averages of 32 trials. To see this figure in color, go online.

dendrite (29). In these experiments, the protocol consisted of two action potentials elicited at 5 ms time intervals (Fig. 7 *a*).

The second action potential was characterized by a decrease in amplitude (Fig. 7 *b*), characteristic of CA1 hippocampal pyramidal neurons (30). This decrease was reflected by a concomitant decrease of the second I_{Ca}/V. Interestingly, the time of the I_{Ca}/V onset in the distal region corresponded to a more hyperpolarized V_m for the second action potential (Fig. 7 *c*), a result consistent in all five cells tested (Fig. 7 *d*). This unexpected result suggested that an additional T-type channel contribution, independent of the initial V_m, was associated with the second action potential. To explore this hypothesis, we tested the delay in the peak of I_{Ca}/V (Δt) produced by the addition of NNC and ML218 (Fig. 7, *e* and *f*). T-type channel blockers delayed the I_{Ca}/V associated with the second action potential, but not that associated with the first action potential, as shown in Fig. 7 *f*. In the six cells tested (Fig. 7 *g*), the delay produced by NNC and ML218 to the second I_{Ca}/V was 0.52 ± 0.09 ms proximally and 0.59 ± 0.09 ms distally. These values were significantly different ($p < 0.01$, two-population *t*-test) from the delays produced by NNC and ML218 to the I_{Ca}/V associated with the first action potential (0.11 ± 0.02 ms proximally and 0.08 ± 0.02 ms distally). These results show that activation and recovery from

inactivation of T-type Ca^{2+} channels during action potentials can be quantitatively investigated together with the V_m and from multiple dendritic sites, using this believed novel approach. Equivalent information cannot be achieved with other existent methods.

DISCUSSION

In this report, we present what we believe to be an original and unique approach that allows the measurement of a local fast Ca^{2+} current from single cells without the constraints of the voltage-clamp technique. In particular, the current can be measured during the physiological change of V_m in combination with the synergistic occurrence of other currents. In the single-electrode voltage-clamp approach, the current measurement is the recording of the total charge flux through the plasma membrane. In contrast, in our method, the measurement consists in the extrapolation of a Ca^{2+} current volume density from the local recording of the concentration of the Ca^{2+} bound to the dye.

The idea of using Ca^{2+} imaging to extract Ca^{2+} flux and to explore Ca^{2+} channels is historical and has been extensively utilized in muscle research (31). Using Ca^{2+} dynamics modeling and Ca^{2+} unitary events, namely Ca^{2+} sparks, Ca^{2+} currents through membranes of intracellular stores were estimated in skeletal muscles (32,33) and cardiac muscles (34). More recently, Ca^{2+} currents through muscular intracellular membranes were estimated using the total fluorescence increase (or signal mass) (35,36). These methods are based on the utilization of the high-affinity indicators Fluo-3 and Fluo-4, which are characterized by a large dynamic range resulting in large changes of fluorescence upon Ca^{2+} increase. Our approach utilizes the low-affinity indicator OG5N, which allows reconstruction of the kinetics of the current at higher temporal resolution. OG5N is used at relatively high concentration (1 mM). Assuming $K_D = 35\ \mu M$ for OG5N, the buffering capacity of the indicator is smaller than the estimated endogenous buffering capacity of the CA1 hippocampal pyramidal neuron dendrite (37). In contrast to the methods developed in the muscle, our method allows us to investigate Ca^{2+} channels expressed in the plasma membrane in combination with patch-clamp recordings and V_m imaging to analyze the voltage dependence of the channels. In this respect, it is crucial to test that Ca^{2+} release from stores is negligible during Ca^{2+} influx, since this possibility may occur during neuronal firing activity (38). Finally, the combined optical measurement of the action potential is also useful in testing whether the measurement is locally affected by photodamage (13).

The quantitative measurement of I_{Ca}/V described here is only the first step toward the use of this method to monitor the distribution of activated Ca^{2+} channels over the cell, since this task will require additional information on the I_{Ca} surface density. The I_{Ca} from a dendritic branch can be simply extracted using the cylindrical approximation of the dendrite. For instance, the current from a dendritic segment of 10 μm with $I_{Ca}/V = 10\ pA/\mu m^3$ and a radius of 1 μm will be 31.4 pA. However, the accurate estimate of the radius cannot be obtained using standard fluorescence microscopy. A more precise radius measurement can be achieved by confocal microscopy, for instance, by taking an image of the dendrite using a spinning disk.

Among the several important applications in which this technique will be relevant, it is worth mentioning the study of activity-dependent modulation of Ca^{2+} channels during physiological activity, the study of functional changes associated with Ca^{2+} channel mutations and pathological conditions, and the implementation of neuron computational models based on optically measured local Ca^{2+} currents. The method is based on the use of a specialized high-speed dual CCD camera, but novel and more economical complementary metal-oxide-semiconductor technology seems to be also suitable for this application (39). Here, to validate the technique, we report an original study of I_{Ca} associated with action potentials recorded at the apical dendrite of CA1 hippocampal pyramidal neurons. Our results show that during an action potential, dendritic high-voltage-activated Ca^{2+} channels always can be activated by V_m depolarization produced by the Na^+ current and are closed by V_m hyperpolarization produced by the K^+ current. In contrast, the opening of T-type channels depends on the state of the channel before the action potential (40). When the cell is not firing, most T-type Ca^{2+} channels are inactivated unless the initial V_m is <-80 mV. However, our results suggest that during firing activity, recovery from inactivation may occur independently of V_m.

CONCLUSION

This approach should drastically improve our understanding of the physiological function of Ca^{2+} channels by making it possible to explore the biophysics of native channels during physiological activity in the subcellular loci of the complex neuronal architecture.

SUPPORTING MATERIAL

Four figures are available at http://www.biophysj.org/biophysj/supplemental/S0006-3495(14)00807-8.

We thank Philippe Moreau for technical help, Jean-Claude Vial for useful discussions, and David Ogden and Joseph Gallagher for reading and revising the manuscript. All experiments were performed at the "Laboratoire Interdisciplinaire de Physique" (LIPhy) at the Joseph Fourier University.

This work was supported by the Agence Nationale de la Recherche (grant Voltimagmicro: program Emergence-10, Labex Ion Channel Science and Therapeutics: program number ANR-11-LABX-0015 and National Infrastructure France Life Imaging Noeud Grenoblois).

REFERENCES

1. Sakmann, B., and E. Neher. 1984. Patch clamp techniques for studying ionic channels in excitable membranes. *Annu. Rev. Physiol.* 46: 455–472.
2. Williams, S. R., and S. J. Mitchell. 2008. Direct measurement of somatic voltage clamp errors in central neurons. *Nat. Neurosci.* 11:790–798.
3. Stuart, G., and N. Spruston. 1995. Probing dendritic function with patch pipettes. *Curr. Opin. Neurobiol.* 5:389–394.
4. Tsien, R. Y. 1989. Fluorescent indicators of ion concentrations. *Methods Cell Biol.* 30:127–156.
5. Canepari, M., and F. Mammano. 1999. Imaging neuronal calcium fluorescence at high spatio-temporal resolution. *J. Neurosci. Methods.* 87:1–11.
6. Kao, J. P., and R. Y. Tsien. 1988. Ca^{2+} binding kinetics of fura-2 and azo-1 from temperature-jump relaxation measurements. *Biophys. J.* 53:635–639.
7. Sabatini, B. L., and W. G. Regehr. 1998. Optical measurement of presynaptic calcium currents. *Biophys. J.* 74:1549–1563.
8. Canepari, M., and D. Ogden. 2006. Kinetic, pharmacological and activity-dependent separation of two Ca^{2+} signalling pathways mediated by type 1 metabotropic glutamate receptors in rat Purkinje neurones. *J. Physiol.* 573:65–82.
9. Woods, C. E., D. Novo, …, J. L. Vergara. 2004. The action potential-evoked sarcoplasmic reticulum calcium release is impaired in mdx mouse muscle fibres. *J. Physiol.* 557:59–75.
10. Antić, S., and D. Zecević. 1995. Optical signals from neurons with internally applied voltage-sensitive dyes. *J. Neurosci.* 15:1392–1405.
11. Jaafari, N., M. Henson, …, M. Canepari. 2013. Economic and simple system to combine single-spot photolysis and whole-field fluorescence imaging. *J. Biomed. Opt.* 18:60505.
12. Canepari, M., K. Vogt, and D. Zecevic. 2008. Combining voltage and calcium imaging from neuronal dendrites. *Cell. Mol. Neurobiol.* 28:1079–1093.
13. Canepari, M., S. Willadt, …, K. E. Vogt. 2010. Imaging inhibitory synaptic potentials using voltage sensitive dyes. *Biophys. J.* 98:2032–2040.
14. Vogt, K. E., S. Gerharz, …, M. Canepari. 2011. High-resolution simultaneous voltage and Ca^{2+} imaging. *J. Physiol.* 589:489–494.
15. Vogt, K. E., S. Gerharz, …, M. Canepari. 2011. Combining membrane potential imaging with L-glutamate or GABA photorelease. *PLoS ONE.* 6:e24911.
16. Savitzky, A., and M. J. E. Golay. 1964. Smoothing and differentiation of data by simplified least squares procedures. *Anal. Chem.* 36:1627–1639.
17. Canepari, M., and K. E. Vogt. 2008. Dendritic spike saturation of endogenous calcium buffer and induction of postsynaptic cerebellar LTP. *PLoS ONE.* 3:e4011.
18. Baylor, S. M., and S. Hollingworth. 2011. Calcium indicators and calcium signalling in skeletal muscle fibres during excitation-contraction coupling. *Prog. Biophys. Mol. Biol.* 105:162–179.
19. Sabatini, B. L., T. G. Oertner, and K. Svoboda. 2002. The life cycle of Ca^{2+} ions in dendritic spines. *Neuron.* 33:439–452.
20. Sutko, J. L., J. A. Airey, …, L. Ruest. 1997. The pharmacology of ryanodine and related compounds. *Pharmacol. Rev.* 49:53–98.
21. Ghosh, T. K., P. S. Eis, …, D. L. Gill. 1988. Competitive, reversible, and potent antagonism of inositol 1,4,5-trisphosphate-activated calcium release by heparin. *J. Biol. Chem.* 263:11075–11079.
22. Bleasdale, J. E., N. R. Thakur, …, S. Bunting. 1990. Selective inhibition of receptor-coupled phospholipase C-dependent processes in human platelets and polymorphonuclear neutrophils. *J. Pharmacol. Exp. Ther.* 255:756–768.
23. Ellis-Davies, G. C., and J. H. Kaplan. 1994. Nitrophenyl-EGTA, a photolabile chelator that selectively binds Ca^{2+} with high affinity and releases it rapidly upon photolysis. *Proc. Natl. Acad. Sci. USA.* 91:187–191.
24. Canepari, M., L. Nelson, …, D. Ogden. 2001. Photochemical and pharmacological evaluation of 7-nitroindolinyl-and 4-methoxy-7-nitroindolinyl-amino acids as novel, fast caged neurotransmitters. *J. Neurosci. Methods.* 112:29–42.
25. Kavalali, E. T., M. Zhuo, …, R. W. Tsien. 1997. Dendritic Ca^{2+} channels characterized by recordings from isolated hippocampal dendritic segments. *Neuron.* 18:651–663.
26. Cueni, L., M. Canepari, …, A. Lüthi. 2009. Ca^{2+} signaling by T-type Ca^{2+} channels in neurons. *Pflugers Arch.* 457:1161–1172.
27. Huang, L., B. M. Keyser, …, M. Li. 2004. NNC 55-0396 [(1*S*,2*S*)-2-(2-(*N*-[(3-benzimidazol-2-yl)propyl]-*N*-methylamino)ethyl)-6-fluoro-1,2,3,4-tetrahydro-1-isopropyl-2-naphtyl cyclopropanecarboxylate dihydrochloride]: a new selective inhibitor of T-type calcium channels. *J. Pharmacol. Exp. Ther.* 309:193–199.
28. Xiang, Z., A. D. Thompson, …, C. W. Lindsley. 2011. The discovery and characterization of ML218: A novel, centrally active T-type calcium channel inhibitor with robust effects in STN neurons and in a rodent model of Parkinson's disease. *ACS Chem. Neurosci.* 2:730–742.
29. Gasparini, S., and J. C. Magee. 2002. Phosphorylation-dependent differences in the activation properties of distal and proximal dendritic Na^{+} channels in rat CA1 hippocampal neurons. *J. Physiol.* 541: 665–672.
30. Andreasen, M., and J. D. Lambert. 1995. Regenerative properties of pyramidal cell dendrites in area CA1 of the rat hippocampus. *J. Physiol.* 483:421–441.
31. Wang, S. Q., C. Wei, …, H. Cheng. 2004. Imaging microdomain Ca^{2+} in muscle cells. *Circ. Res.* 94:1011–1022.
32. Klein, M. G., H. Cheng, …, M. F. Schneider. 1996. Two mechanisms of quantized calcium release in skeletal muscle. *Nature.* 379:455–458.
33. Tsugorka, A., E. Ríos, and L. A. Blatter. 1995. Imaging elementary events of calcium release in skeletal muscle cells. *Science.* 269: 1723–1726.
34. Shkryl, V. M., L. A. Blatter, and E. Ríos. 2012. Properties of Ca^{2+} sparks revealed by four-dimensional confocal imaging of cardiac muscle. *J. Gen. Physiol.* 139:189–207.
35. ZhuGe, R., K. E. Fogarty, …, J. V. Walsh, Jr. 2000. Dynamics of signaling between Ca^{2+} sparks and Ca^{2+}- activated K^{+} channels studied with a novel image-based method for direct intracellular measurement of ryanodine receptor Ca^{2+} current. *J. Gen. Physiol.* 116:845–864.
36. Zou, H., L. M. Lifshitz, …, J. J. Singer. 2004. Using total fluorescence increase (signal mass) to determine the Ca^{2+} current underlying localized Ca^{2+} events. *J. Gen. Physiol.* 124:259–272.
37. Maravall, M., Z. F. Mainen, …, K. Svoboda. 2000. Estimating intracellular calcium concentrations and buffering without wavelength ratioing. *Biophys. J.* 78:2655–2667.
38. Sandler, V. M., and J. G. Barbara. 1999. Calcium-induced calcium release contributes to action potential-evoked calcium transients in hippocampal CA1 pyramidal neurons. *J. Neurosci.* 19:4325–4336.
39. Davies, R., J. Graham, and M. Canepari. 2013. Light sources and cameras for standard in vitro membrane potential and high-speed ion imaging. *J. Microsc.* 251:5–13.
40. Kuo, C. C., and S. Yang. 2001. Recovery from inactivation of t-type Ca^{2+} channels in rat thalamic neurons. *J. Neurosci.* 21:1884–1892.

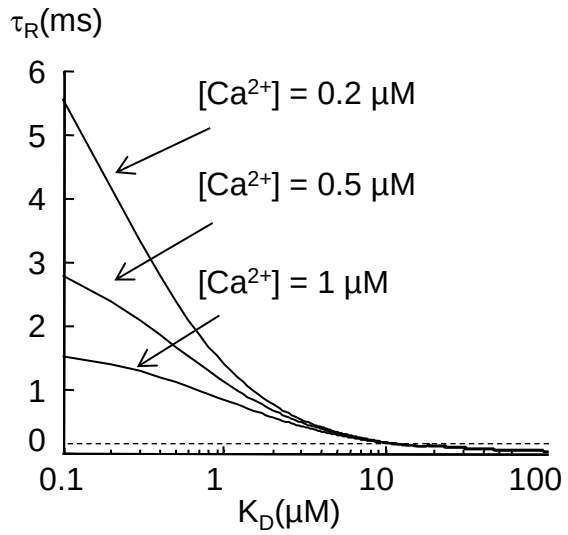

Figure S1 Relaxation time (τ_R) of the Ca^{2+}-dye binding reaction against the equilibrium constant (K_D) of the indicator according to the Kao and Tsien equation (equation 1 in the main text). The association constant (K_{ON}^{Dye}) of the indicator is set to $6 \cdot 10^8$ $M^{-1}s^{-1}$. The three plots correspond to the values of $[Ca^{2+}]$ of 0.2, 0.5 and 1 µM. The dotted line indicates the K_D above which τ_R is always <150 µs (~10 µM). Notice that this limit does not depend on $[Ca^{2+}]$.

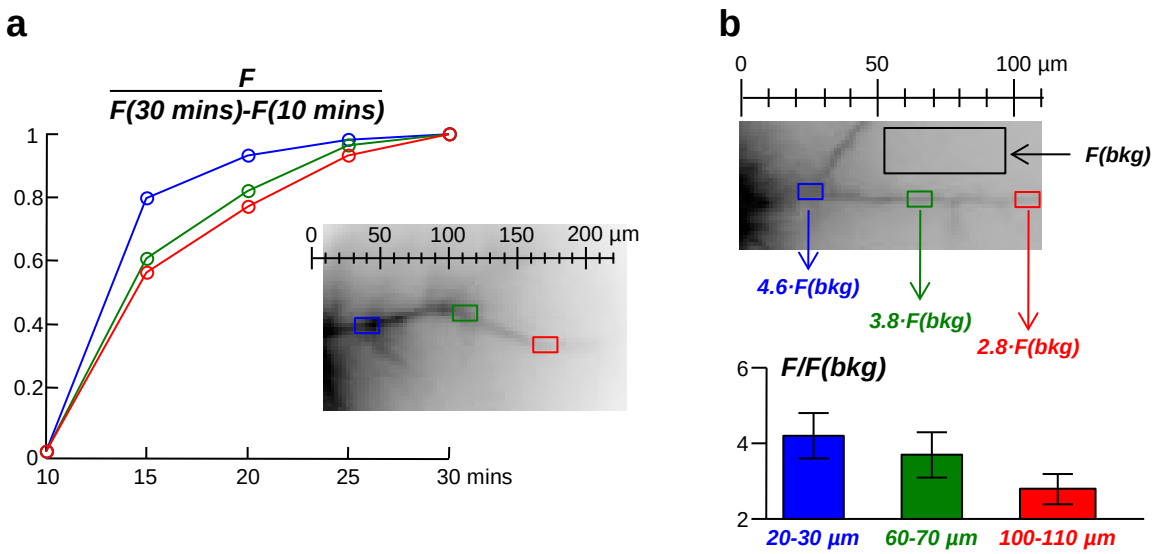

Figure S2 Equilibration of the indicator in the apical dendrite and estimate of the autofluorescence. (***a***) Fluorescence at 10, 15, 20, 25 and 30 minutes after establishing the whole-cell normalised to the difference between fluorescence 30 minutes after whole-cell and 10 minutes after whole cell; blue, green and red lines and symbols are from regions 30-50 µm, 100-120 µm and 160-180 µm from the soma respectively; fluorescence recorded 10 minutes after whole-cell was always between 20 % and 50 % of the fluorescence recorded 30 minutes after whole cell in the initial 200 µm segment of the apical dendrite. (***b***) Top: Image of the initial segment of a CA1 hippocampal pyramidal neuron filled with 1 mM OG5N; the image was acquired ~25 minutes after the establishment of the whole-cell configuration; the black rectangle indicates a region where the light intensity acquired by the camera was averaged to estimate the autofluorescence background, defined as *F(bkg)*; the blue, green and red rectangles limit three dendritic regions from where light intensity was estimated with respect to *F(bkg)* as indicated below. Bottom: Mean ± SD of the ratio between dendritic fluorescence at 20-30 µm (blue column / 4.4 ± 0.6), at 60-70 µm (green column / 3.7 ± 0.6) and at 100-110 µm (red column / 2.8 ± 0.4) from the soma.

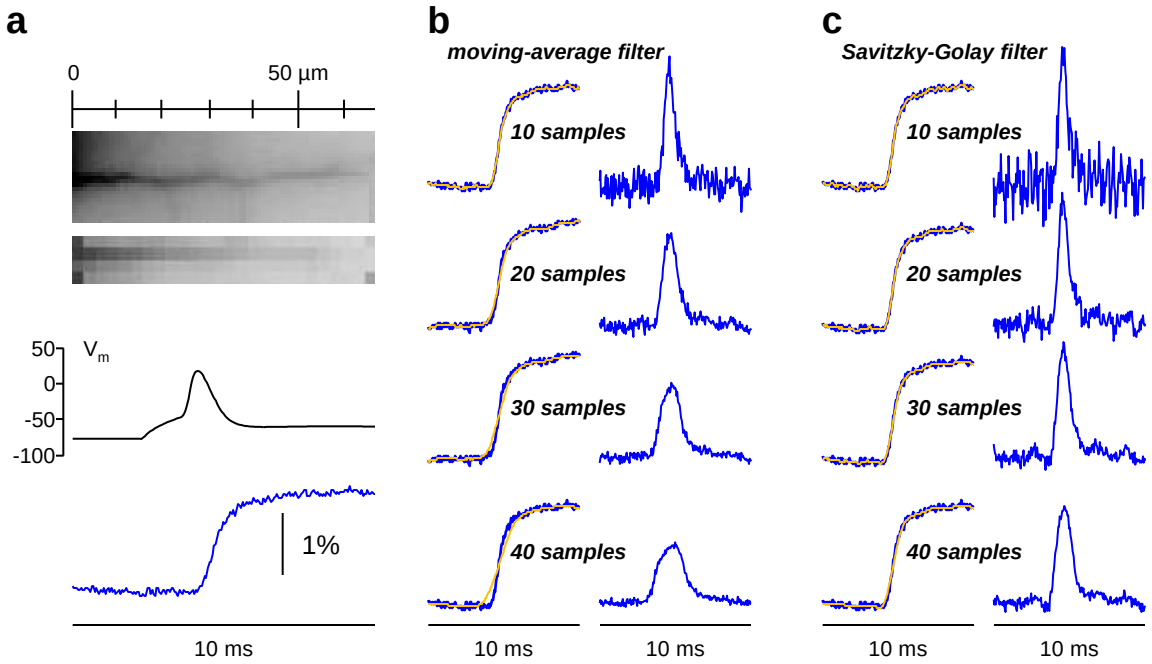

Figure S3 Comparison of different smoothing filters. Temporal filtering distorts $\Delta F/F_0$ and therefore its time-derivative if the time-window of the temporal filtration is too large. To minimise this problem one can use a filtering approach called "smoothing". The figure shows the comparison between a moving average filter and a Savitzky-Golay filter, both implemented by the "smooth" function in the Matlab "Curve Fitting Toolbox". The moving-average filter consists in the replacement of each data point with the average of the neighboring data points defined within the number of samples. In contrast, the Savitzky-Golay filter consists in a moving-average algorithm where the filter coefficients are derived by performing weighted linear least-squares fit. This filter has worse performance in improving the S/N for the same number of samples, but it significantly reduces the distortion for the same number of samples. (***a***) Top: Ca^{2+} fluorescence images of initial segment of an apical dendrite including the sub-image acquired at 20 kHz. Bottom: OG5N-$\Delta F/F_0$ signal (blue trace) associated with an AP (black trace) averaged over 32 trials from the entire field of view. (***b***) Left: the same OG5N-$\Delta F/F_0$ signal (blue) superimposed to the filtered traces (yellow) using a moving-average algorithm consisting in the replacement of each data point with the average of the neighboring data points defined within the number of samples (indicated); different time-windows (10, 20, 30 or 40 samples) were tested; the algorithm is implemented by the "smooth" function in the Matlab "Curve Fitting Toolbox". Right: time-derivatives of the filtered traces. (***c***) Same as *b* but using the Savitzky-Golay filter algorithm implemented by the "smooth" function in the Matlab "Curve Fitting Toolbox"; this filter consists in a moving-average algorithm where the filter coefficients are derived by performing unweight linear least-squares fit; notice that for 10 samples the filtered traces obtained with the two filters have the same time-course of the original trace but the time-derivative associated with the Savitzky-Golay filter is noisier; however, for larger time-windows, the filtered traces obtained with the moving-average filter, but not those obtained with the Savitzky-Golay filter, produce a distortion with respect to the original trace; thus, the Savitzky-Golay filter using time windows of 20- 40 samples preserves the time course of the Ca^{2+} current with minimal noise.

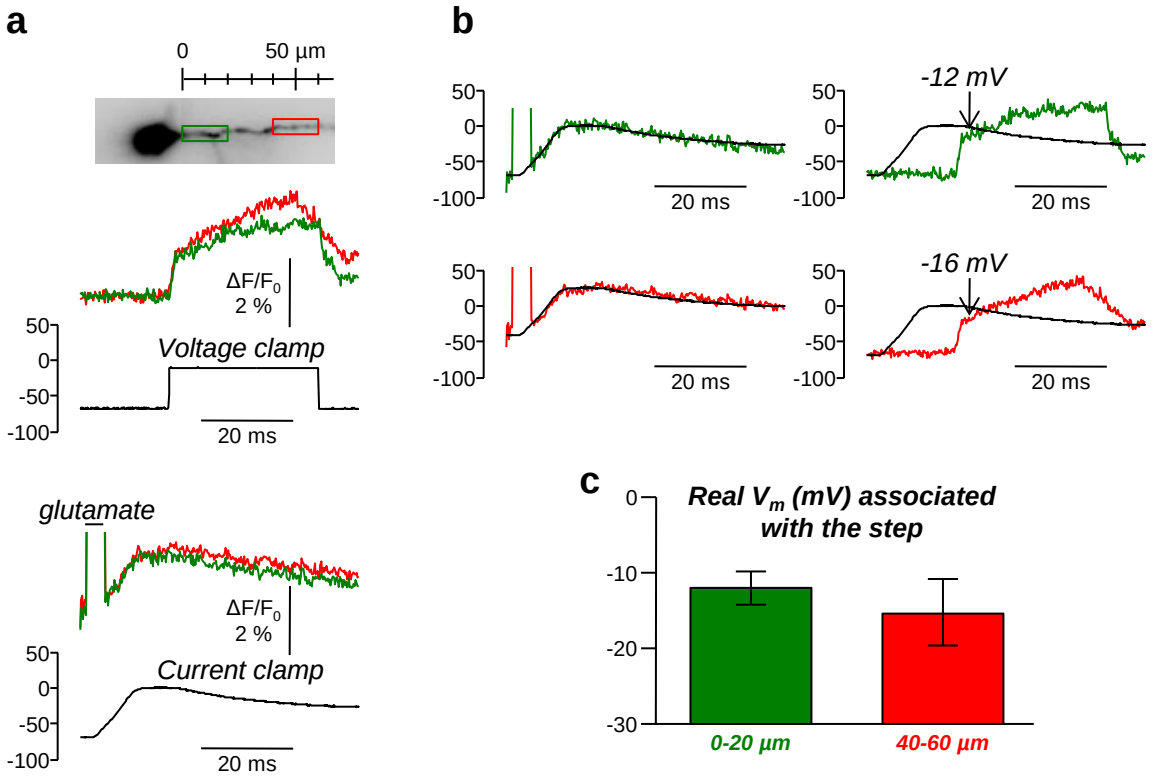

Figure S4 V_m optical measurement of the real membrane potential reached in the initial 60 µm segment of the apical dendrite during a step, in voltage clamp, from -70 mV to -10 mV, in the presence of Na^+ and K^+ channels blockers (1 µM tetrodotoxin, 5 mM TEA, 4 mM 4-aminopyridine extracellularly and 5 mM TEA intracellularly). Four CA1 hippocampal pyramidal neurons were filled with the voltage sensitive dye JPW1114; fluorescence was excited at 532 nm and images were taken at 5kHz. V_m signals were associated either with a 32 ms voltage step from -70 mV to -10 mV in voltage clamp or with a glutamate photorelease from the caged compound MNI-glutamate. The second protocol was used for calibration of the first. (***a***) Top: Image of the initial segment of the apical dendrite of a neuron; green and red rectangles limit two regions 0-20 µm and 40-60 µm from the soma respectively. Middle-bottom: fluorescence changes associated with the two protocols described above; green and red traces correspond to the two regions of interest indicated in the top image. (***b***) Left: scaling of the fluorescence associated with glutamate photorelease with respect to somatic recording. Right: the same scaling is used to calibrate the fluorescence change associated with the voltage step; the arrows indicate the V_m reached 4 ms after the beginning of the step; the conductance opening prevents clamping the dendrite at -10 mV for longer durations. (***c***) The mean ± SD of V_m reached 4 ms after the beginning of the step from the four cells tested; green (-12.0 ± 2.2 mV) and red (-15.4 ± 4.4 mV) columns correspond to the two regions 0-20 µm and 40-60 µm from the soma respectively. Data were averages of four recordings.